

VLA Observations of the AE Aqr-type Cataclysmic Variable LAMOST J024048.51+195226.9

PAUL E. BARRETT¹

¹*Department of Physics, The George Washington University, Washington, DC 20052 USA*

ABSTRACT

AE Aqr was until recently the only known magnetic cataclysmic variable (MCV) containing a rapidly spinning (33.08 s) white dwarf (WD). Its radio emission is believed to be a superposition of synchrotron emitting plasmoids, because it has a positive spectral index spanning three orders of magnitude ($\approx 2 - 2000$ GHz) and is unpolarized. Both characteristics are unusual for MCVs. Recently, Thorstensen has suggested that the cataclysmic variable LAMOST J024048.51+195226.9 (henceforth, J0240+19) is a twin of AE Aqr based on its optical spectra. Optical photometry shows the star to be a high-inclination, eclipsing binary with a spin period of 24.93 s, making it the fastest spinning WD. This paper presents three hours of Very Large Array radio observations of J0240+19. These observations show that the persistent radio emission from J0240+19 is dissimilar to that of AE-Aqr in that it shows high circular polarization and a negative spectral index. The emission is most similar to the nova-like CV V603 Aql. We argue that the radio emission is caused by a superposition of plasmoids emitting plasma radiation or electron cyclotron maser emission from the lower corona of the donor star and not from the magnetosphere near the WD, because the latter site is expected to be modulated at the orbital period of the binary and to show eclipses of which there is no evidence. The radio source J0240+19, although weak ($\lesssim 1$ mJy), is a persistent source in a high-inclination eclipsing binary, making it a good laboratory for studying radio emission from CVs.

Keywords: Cataclysmic variable stars; Intermediate Polars; White dwarf stars; Magnetic stars; AE Aquarii; Astronomy; Radio

1. INTRODUCTION

Magnetic cataclysmic variables (MCVs) showing two photometric periods are called Intermediate Polars (IPs, aka DQ Herculis stars). The longer period (of order a few hours) is associated with the orbital period P_{orb} of the binary and the shorter period (of order tens of minutes) with the rotation period P_{rot} of the white dwarf (WD). The ratio $P_{rot}/P_{orb} \approx 0.1$. The exception to the spin-orbit rule is AE Aquarii (AE Aqr), which until recently, contained the fastest known rotating WD with a period of 33.08 s ($P_{rot}/P_{orb} \approx 0.001$; [Patterson 1979](#)). The rapid rotation along with the moderately strong magnetic field of the WD (1-10 MG) causes almost all of the accreted material ($\sim 99.9\%$; [Meintjes et al. 2015](#)) to be expelled from the binary in a so called “magnetic propeller”. The WD’s rapidly spinning magnetosphere acts as a centrifugal barrier to the accreted diamagnetic plasmoids and propels them out of the system ([Wynn & King 1995](#); [Wynn et al. 1997](#)). This accretion scenario is similar to that of accreting millisecond pulsars.

AE Aqr also has several other unique observational characteristics. [de Jager et al. \(1994\)](#) using 14 years of X-ray data found that the WD is spinning down at a rate of $\dot{P}_\star \approx 5.64 \times 10^{-14}$ s s⁻¹. This rate equates to a spin-down luminosity $L_{s-d} = I\dot{\Omega} \sim 10^{34}$ erg s⁻¹. This is roughly 500 times larger than the accretion luminosity of 2×10^{31} erg s⁻¹ ([Eracleous & Horne 1996](#)).

[Bookbinder & Lamb \(1987\)](#) and [Bastian et al. \(1988\)](#) using the Very Large Array found that AE Aqr is a persistent radio emitter showing rapid variability and large flares. Observations at 1.5, 4.9, 15, and 22.5 GHz show a long-term averaged spectral index $\alpha \propto 0.5$ ($S_\nu \propto \nu^\alpha$; [Bastian et al. 1988](#)). The flux density at 15 GHz showed variations of a few mJy on minute timescales during quiescence and peaked at 12 mJy during flares, which occur about every five hours. They also note that in those cases where the flares are temporally resolved, the rise time is shorter than the decay time, which suggests that an external medium limits the flare’s rate of expansion. Ground-based millimeter and submillimeter, and spaced-based infrared observations show that the positive spectral index extends to THz frequencies

(Abada-Simon *et al.* 2005; Dubus *et al.* 2007; Torkelsson 2013). Above 2 THz the spectrum turns over and has a spectral index of $\alpha \propto -0.7$. This nonthermal radio emission, spanning more than three orders of magnitude in frequency, is attributed to a superposition of synchrotron emitting plasmoids that expand and cool radiatively through synchrotron radiation (van der Laan 1963, 1966).

Thorstensen (2020) recently argued that the CV LAMOST J024048.51+195226.9, aka as CRTS J024048.5+19227, (hereafter J0240+19) may be a possible twin of AE Aqr based on its unusual optical spectrum, which shows no He II emission and weak He I lines. In addition, the light curves show large irregular flaring on the timescale of minutes. However, the time resolution of the photometry was insufficient to search for pulsations on the order of tens of seconds. Using publically available Catalina Real-Time Transient Survey (CRTS) and All-Sky Automated Survey for Supernovae (ASAS-SN) data, Littlefield & Garnavich (2020) identify a shallow dip in the light curves at the secondary’s inferior conjunction and identify this feature with an eclipse by the secondary star. This means that J0240+19 is a high inclination system and explains why the He I $\lambda 6678$ Å emission line briefly disappears at orbital phase 0. Additional photometric observations by Garnavich *et al.* (2021) confirmed the high inclination of J0240+19, but did not detect the WD’s spin period. The spin period was finally found by Pelisoli *et al.* (2021) to be 24.9328(38) s with an amplitude of 0.2% in the *g*-band, which is below the detection limits of the previous searches. J0240+19 is now the fastest known rotating WD. A search of the NRAO Very Large Array Sky Survey (VLASS) version 1.2 (sp., tile T15t04, dated 2019-06-07; Lacy *et al.* 2020) showed the presence of a 508 ± 120 μ Jy (4σ) radio source at 3 GHz within 1 arcsec of the J0240+19 position. It was also detected in a MeerKAT pointed observation on 2020-08-12 with a flux density of 600 ± 20 μ Jy at 1.284 GHz and spectral index $\alpha \propto -0.6$ (Pretorius *et al.* 2021). Neither observation reported any polarization measurements.

In this paper we present three hours of National Radio Astronomy Observatory (NRAO) *Karl G. Jansky* Very Large Array (VLA) observations of J0240+19. The observations are split between one hour of spectroscopy in order to compare the spectrum of J0240+19 to that of AE Aqr and two hours of photometry in order to detect the spin period of the WD. If J0240+19 is a twin of AE Aqr, then its radio flux density is expected to increase with frequency and to be ≈ 1.4 mJy at 22 GHz, assuming a flux density of 508 μ Jy at 3 GHz and a spectral index of 0.5, the same as AE Aqr. At this flux density, it should be possible to detect a large amplitude pulsation with a period as short as 30 s.

2. OBSERVATIONS & DATA REDUCTION

J0240+19 was observed by the VLA for three hours on two separate dates. The first observation measured the spectrum of J0240+19 across five radio bands from 2–26 GHz during a one hour scheduling block. The exposures in each band range between 600–628 s duration. The results of this observation determined which frequency band to use for the second photometric observation of two hours. This second observation was done using the C-band (4–8 GHz) with an on-source time of about 1.6 hours. During the second observation, the VLA cycled between the target J0240+19 and the phase calibrator J0238+1636 every 570 s with about 525 s being on target. Each observation used the 3-bit samplers for wideband coverage. The radio sources J0137+3309 (=3C48) and J0238+1636 were used as the flux and polarization, and the phase and gain calibrators for each observation, respectively. No polarization leakage calibrators were observed, because the cross-polarization is $< 1\%$ and varies slowly over several months (Perley & Sault 2014). This accuracy is sufficient for our needs. Note that the flux calibrator 3C48 has been undergoing a flare since about January 2018, which will affect the absolute flux scale. The effect is smaller at low frequencies ($\sim 5\%$ at S-band) and greater at high frequencies ($\sim 10\%$ at Ku-band; VLA SUS 2021). Table 1 gives a log of the observations.

The data were calibrated using version 6.1.2 of the CASA (Common Astronomy Applications Software) calibration pipeline (McMullin *et al.* 2007). The imaging application *tclean* is used to generate IQUV and RRLL images of each target scan to check for any source confusion and radio frequency interference. None were found. The flux densities are measured by fitting a point source to the UV data using the Julia programming language package *Visfit* (Barrett 2021). The package uses a box-constrained Levenberg-Marquardt algorithm to minimize the model residuals. The position of the point source is constrained to be within ± 2 arcsec of the known source position. When measuring the left and right circular polarizations, the flux densities are measured simultaneously using the same source position. Although the phase centers for the left and right polarizations may have slightly different positions, this approach is recommended for faint sources.

3. ANALYSIS

Table 1. Log of the observations of J0240+19.

Start Date	Start Time	Band	Frequency	Exposure
	(UTC)		(GHz)	(h:m:s)
2021 Jun 11	16:52:36	K	18–26	00:05:28
	16:59:54	Ku	12–18	00:05:22
	17:07:09	X	8–10	00:05:12
	17:14:15	C	4–8	00:05:10
	17:21:20	S	2–4	00:05:00
2021 Jul 20	15:22:50	C	4–8	01:35:55

3.1. Spectroscopy

The spectrum of J0240+19 obtained during the first observation is shown in Figure 1. This observation occurred between orbital phases 0.70–0.78 using the ephemeris of [Garnavich *et al.* \(2021\)](#). The average flux density and standard deviations for each frequency band are shown in black. It varies from $195 \pm 12 \mu\text{Jy}$ at 3 GHz to $23 \pm 8 \mu\text{Jy}$ at 22 GHz. The spectral index of these measurements is roughly consistent with the negative spectral index measured by MeerKAT of $\alpha \propto -0.6$ ([Pretorius *et al.* 2021](#)), where $S_\nu \propto \nu^\alpha$. Figure 1 also shows the left (LL) and right (RR) circular polarizations for a narrower bandwidth (512 MHz) across the entire frequency range. These data show that the circular polarization varies randomly from one frequency to the next. In particular, the measurement at 4.231 GHz shows strong ($> 50\%$) circularly polarized emission. Note that the Q and U images show no significant linear polarization ($\lesssim 1\%$).

3.2. Photometry

Because the spectroscopy showed that the S and C bands have similar flux densities ($\approx 200 \mu\text{Jy}$), the photometry was done using the C band, because its wider bandwidth provides greater sensitivity. Unfortunately, J0240+19 was even weaker during the second observation with an average flux density of $\approx 100 \mu\text{Jy}$. Such a low flux density precludes any attempt at searching for, or detecting, a spin period as short as 30 s. We found that the best compromise between time resolution and signal-to-noise ratio is an integration time of 265 s. The observation occurred just after inferior conjunction between orbital phases 0.08–0.32 using the ephemeris of [Garnavich *et al.* \(2021\)](#). The resulting left and right circular polarization light curves are shown in Figure 2. Like the spectrum shown in Figure 1, the light curve also shows that the flux density and circular polarization vary randomly on a timescale of at most a few minutes. The light curve is too short and variable to show any evidence of an orbital period.

4. DISCUSSION

4.1. Coherent radio emission

The brightness temperature, $T_B \approx 10^{14} S_{-3} D_2 \nu_9^{-2} r_{10}^{-2}$ K, where S_{-3} is the observed flux density in mJy, D_2 is the distance in units of 100 pc, ν_9 is the frequency in GHz, and r_{10} is the radius of the projected source area in 10^{10} cm. For J0240+19, $T_B \approx 10^{13}$ K for $S_{-3} = 0.2$ at 3 GHz, $D = 6.2$ ([Gaia Collab. 2020](#)), and $r_{10} = 7$. The value of r_{10} assumes that the area of the radio emission has a radius twice that of the donor star. This high T_B implies a coherent emission process.

Following the discussion of [Bastian & Bookbinder \(1987\)](#), there are two coherent mechanisms that can produce highly circularly polarized emission as seen in the spectrum and light curve of J0240+19: magnetic plasma radiation and electron cyclotron maser emission (ECME). Synchrotron emission as suggested by ([Pretorius *et al.* 2021](#)) is unlikely. These emissions can be produced by the ordinary (O), the extraordinary (X), or the low frequency branch of the extraordinary (Z) modes depending on the emission mechanism. In the case of plasma emission, the radiation is produced at either the fundamental or the second harmonic of the electron plasma frequency, $\omega_{pe} = (4\pi n_e e^2 / m_e)^{1/2}$, where n_e is the electron density, e is the electron charge, and m_e is the electron mass. Emission at the fundamental frequency can be completely polarized and is ascribed to the O-mode. Whereas, emission at the second harmonic is

LAMOST J0240+19 spectrum

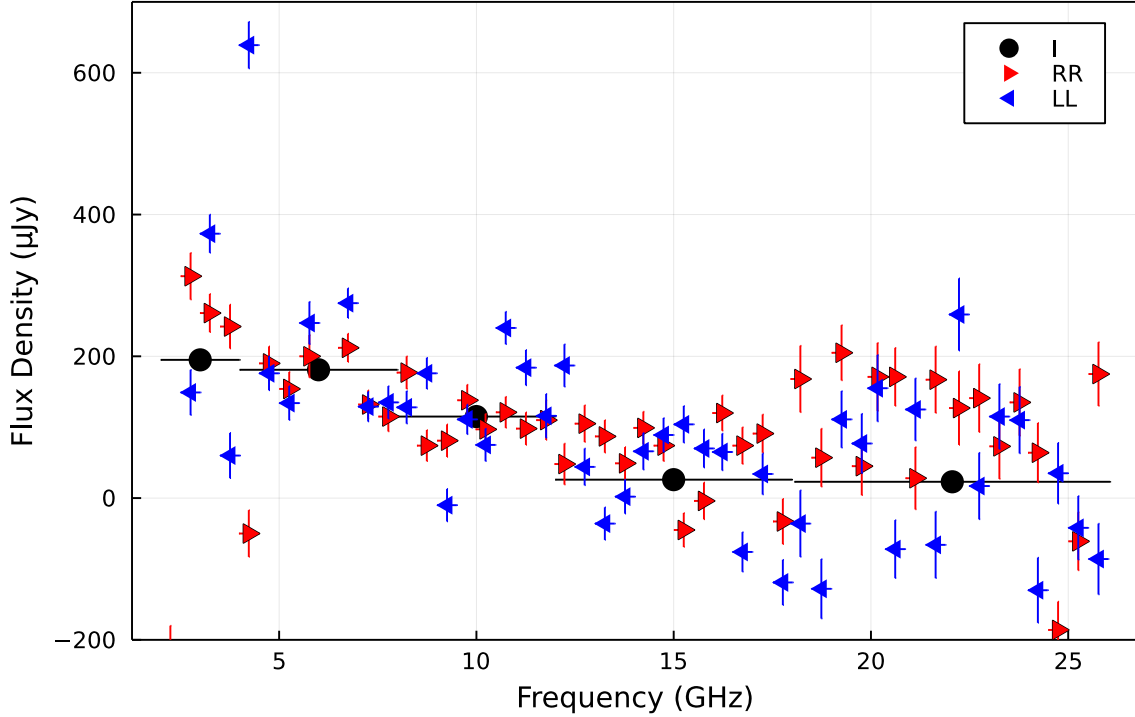


Figure 1. 2–26 GHz spectrum of LAMOST J0240+19. The average flux densities (black points) are shown for each of the five spectral bands (S, C, X, Ku, & K). The left (blue) and right (red) circular polarizations are also shown for a narrower bandwidth (512 MHz). Note the high polarization at 4.231 GHz.

moderately polarized and is related to either the O- or X-modes. For the frequency range of 2–18 GHz, ω_{pe} gives a density of the source region of $\approx 10^9 - 10^{11} \text{ cm}^{-3}$.

In the case of ECME, the polarized emission is related to the O-, X-, or Z-modes. Emission at the fundamental gyrofrequency, $\Omega_{Be} = eB/m_e c$, is unlikely to escape the source region, because of the strong gyroresonant absorption at the second harmonic. However, emission at the second harmonic of the O- or X-modes may escape the source region and be highly polarized. The polarized emission at ≈ 2 GHz places an upper limit of $\lesssim 4 \times 10^{10} \text{ cm}^{-3}$ on the electron density, since the ECME requires the plasma frequency to be less than the gyrofrequency. It also implies that the ambient magnetic field of the source region B ($\approx 2.8 (\frac{B}{1 \text{ G}})$ MHz) is in the range of 360 – 3200 G.

4.2. The radio emission compared to AE Aqr

The two physical constraints of a low density plasma and kiloGauss magnetic field restricts the location of the radio emission to a low density plasma in the magnetosphere of the WD or the lower corona of the donor star. Emission from the accretion stream or disk is therefore unlikely because the densities in those regions are too high ($\gtrsim 10^{14} \text{ cm}^{-3}$ Barrett *et al.* 2020). We first consider emission from the WD magnetosphere. Assuming a 1 MG dipolar surface field for the WD, The strength of the magnetic field with radius is: $B = 10^6 r_9^{-3} \text{ G}$, where r_9 is the WD radius in 10^9 cm . Therefore, the radio emission comes from a region between 7–14 WD radii for magnetic fields of 360–3200 G. These radii are much smaller than the radius of the donor star and are therefore likely to be modulated by the orbital period and eclipsed by the donor star. Although the radio observations are sparse and do not cover the orbital phase of the eclipse (0.95–0.05), neither the MeerKAT L-band (Pretorius *et al.* 2021) nor VLA C-band observations show any evidence of an orbital modulation. The MeerKAT observations occur during orbital phases 0.25–0.44 and our VLA observation during phases 0.08–0.32. Therefore, emission from the WD magnetosphere is problematic.

Based on these arguments, the donor star’s corona is the most likely location of the radio emission. Roche tomography of the donor star of AE Aqr (Dunford & Smith 2005; Watson *et al.* 2006; Smith *et al.* 2012) shows that $\sim 20\%$ of its surface is affected by high-latitude starspots similar to that seen in Doppler images of rapidly rotating isolated stars. This implies that the donor star in AE Aqr is highly active, which is expected for a rapidly rotating star ($P_{rot} < 10$

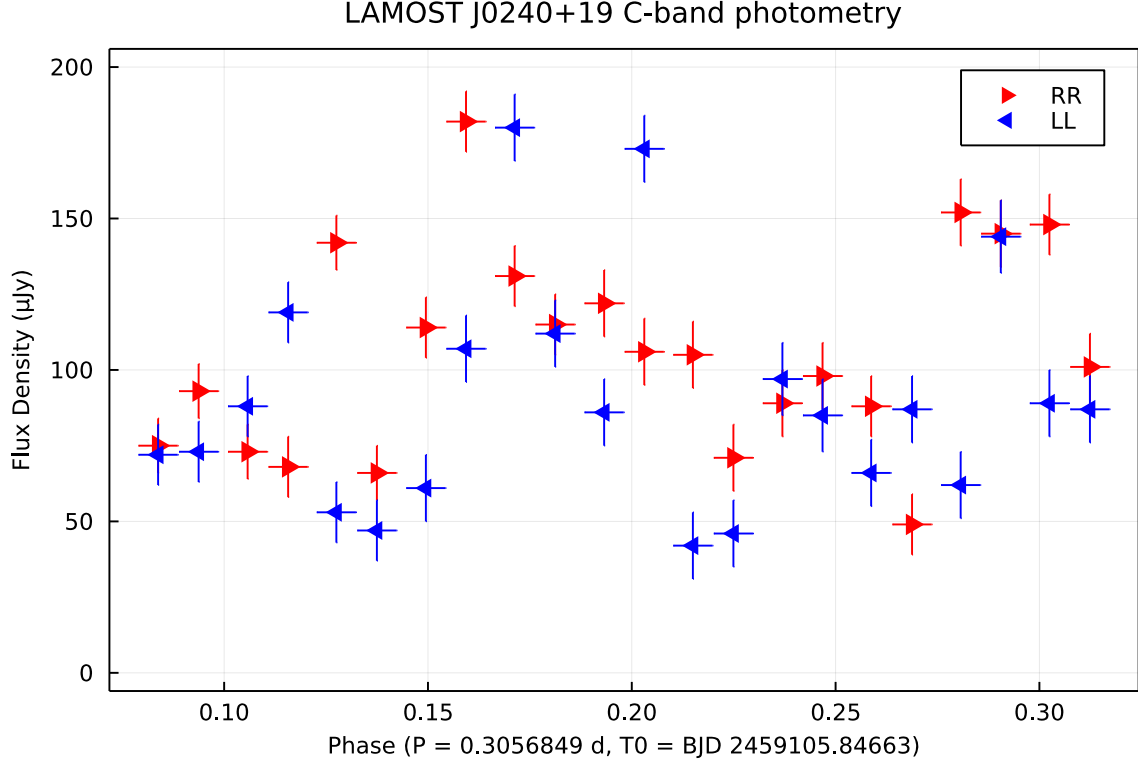


Figure 2. 1.6 hours of C-band photometry (4–8 GHz) of LAMOST J0240+19. The left (blue) and right (red) circular polarization are shown. The integration time for each flux measurement is 265 s.

days), because the magnetic dynamo saturates at about this spin period. We propose that the donor star in J0240+19 is also magnetically active and is the source of the radio emission. This means that the surface field of the donor star is \sim few kG in strength. It also provides an explanation of the random nature of the circular polarization in time and frequency due to a superposition of plasma radiation or ECME from several emitting plasmoids.

In order to compare the spectra of AE Aqr and J0240+19, we have reanalyzed one of the observations of AE Aqr by Barrett *et al.* (2017) from 2015. Figure 3 shows a positive spectral index between the C- and K-bands (6 GHz & 22 GHz, resp.). Because each band was observed several minutes apart and the radio emission varies rapidly (\sim minutes), the X-band (8 GHz) was caught during a period of negative spectral index. As noted previously, AE Aqr has a positive spectral index spanning over three orders of magnitude and only begins to turnover at ≈ 2 THz. Also note that radio emission in all three bands is unpolarized ($P_V \lesssim 0.1\%$). This spectrum is unlike that of the spectrum of J0240+19 with its negative spectral index and strong circular polarization. Instead, the spectrum of J0240+19 is similar to that of the nova-like V603 Aql, which on average has a negative spectral index between 2–12 GHz and shows strong, randomly varying, circular polarization (Coppejans *et al.* 2015; Barrett *et al.* 2017, 2020, 2021)¹. In addition, the specific radio luminosities at 3 GHz are of similar magnitude. That of J0240+19 is $7.3\text{--}18.3 \times 10^{15} \text{ ergs s}^{-1} \text{ Hz}^{-1}$ and that of V603 Aql is $2.0\text{--}3.5 \times 10^{15} \text{ ergs s}^{-1} \text{ Hz}^{-1}$. These luminosities are in the range of $1\text{--}50 \times 10^{15} \text{ ergs s}^{-1} \text{ Hz}^{-1}$, which is typical of most CVs (See Figure 2 of Pretorius *et al.* 2021).

5. CONCLUSIONS

The three hours of VLA observations of J0240+19 show a spectrum and light curve that are dissimilar to those of AE Aqr. The spectrum has a negative spectral index between 2–26 GHz and the emission shows periods of high circular polarization, while those of AE Aqr show a positive spectral index and unpolarized emission. The radio emission from J0240+19 is characteristic of magnetic plasma radiation or electron cyclotron maser emission, while that of AE Aqr and AR Sco is characteristic of synchrotron emission. Therefore, the radio emission from J0240+19 is unlike that of

¹ Although, V603 Aql has been suspected of being an IP, to date no optical or X-ray spin period has been detected (see e.g., Haefner & Metz 1985; Udalski & Schwarzenberg-Czerny 1989; Gnedin *et al.* 1990)

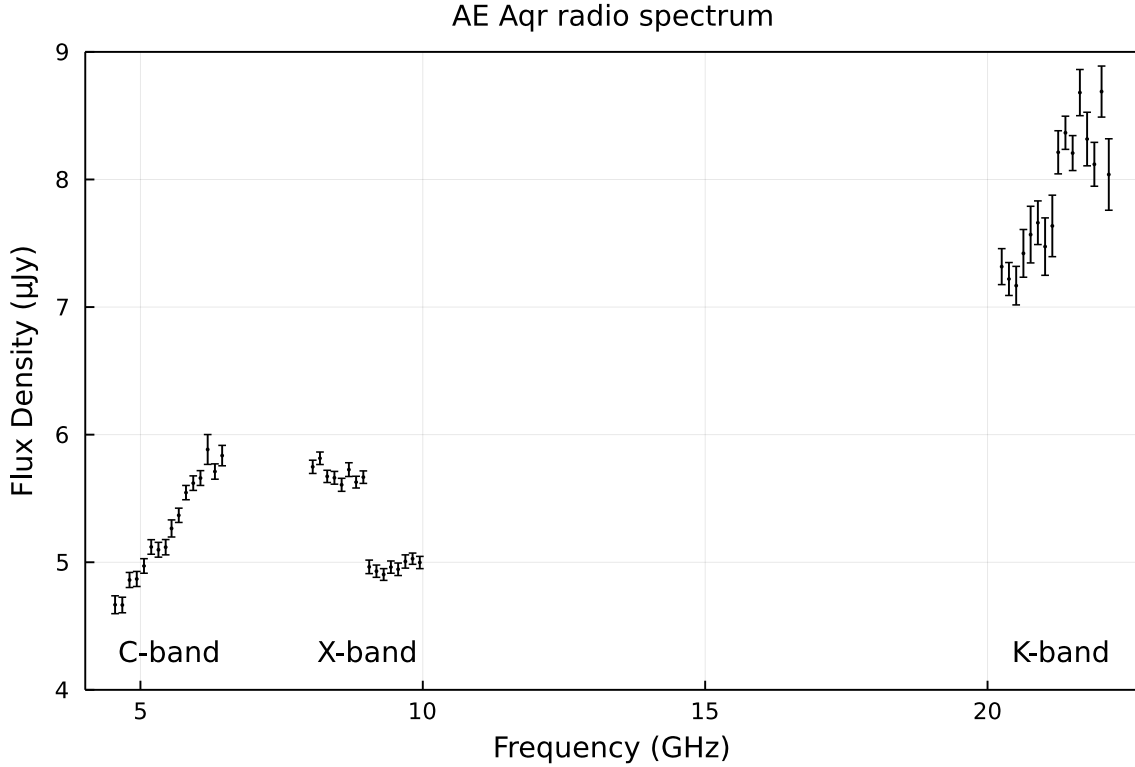


Figure 3. The 4-24 GHz spectrum of AE Aqr showing a positive spectral index between the C- and K-bands.

AE Aqr and AR Sco, although the characteristics of their optical emission are very similar. The radio emission from J0240+19 is similar to most radio-emitting magnetic CVs and is most similar to the nova-like CV V603 Aql, which is suspected of containing a rapidly spinning WD.

We argue that the source of the radio emission in J0240+19 is the magnetically active donor star and not a low density region of the magnetosphere near the WD, because the radio light curves show no evidence of an orbital modulation. If the radio emission is from the WD magnetosphere, then it should be eclipsed during inferior conjunction, because of its proximity to the WD. We therefore encourage additional radio observations to refute this assertion by looking for radio eclipses. Although J0240+19 is a weak radio source ($\lesssim 1$ mJy), it is a persistent source in a high-inclination, eclipsing CV, making it a good laboratory for studying radio emission from CVs.

6. ACKNOWLEDGEMENTS

We thank Paul Mason for a critical reading of the manuscript and several useful comments. The National Radio Astronomy Observatory is a facility of the National Science Foundation operated under cooperative agreement by Associated Universities, Inc.

REFERENCES

- | | |
|---|---|
| Abada-Simon, M., <i>et al.</i> 2005, A&A, 433, 1063. | Bastian, T. S., Dulk, G. A., & Chanmugam, G. 1988, ApJ, 324, 431. |
| Barrett, P. E., Dieck, C., Beasley, A. J., Singh, K. P., & Mason, P. A. 2017, AJ, 154, 252–260. | Bookbinder, J. A. & Lamb, D. Q. 1987, ApJ, 323, L131. |
| Barrett, P., Dieck, C., Beasley, A. J., Mason, P. A., & Singh, K. P. 2020, AdSpR, 66, 1226. | Coppejans, D. L., Körding, E. G., Miller-Jones, J. C. A., Rupen, M. P., Knigge, C., Sivakoff, G. R., & Groot, P. J. 2015, MNRAS, 451, 3801. |
| Barrett, P. 2021, in preparation. | de Jager, O. C., Meintjes, P. J., O’Donoghue, D., & Robinson, E. L. 1994, MNRAS, 267, 577. |
| Barrett, P., Dieck, C., Beasley, A. J., Mason, P. A., & Singh, K. P. 2021, in preparation. | |
| Bastian, T. S. & Bookbinder, J. A. 1987, Nature, 326, 678. | |

- Dunford, A. & Smith, R. C. 2005, ASPConf (eds. Hameury & Lasota), 330, 399.
- Dubus, G., Taam, R. E., Hull, C., Watson, D. M., & Mauerhan, J. C. 2007, ApJ, 663, 516.
- Eracleous, M. & Horne, K. 1996, ApJ, 471, 427.
- Gaia Collaboration, Brown, A. G. A., Vallenari, Prusti, A. T., de Bruijne, J. H. J., Babusiaux, C., & Biermann, M. (2020), arXiv 2012.01533.
- Garnavich, P., Littlefield, C., Wagner, R. M., van Roestel, J., Jaodand, A. D., Szkody, P., & Thorstensen, J. R. 2021, ApJ, 917, 22.
- Gnedin, Y. N., Borisov, N. V., & Natsvlshvili, T. M., 1990, Soviet Astro Let, 16, 272.
- Haefner, R. & Metz, K. 1985, A&A, 145, 311.
- Lacy, M., Baum, S. A., Chandler, C. J., Clarke, T. E., Deustua, S., *et al.*, 2020, PASP, 132, 1.
- Littlefield, C. & Garnavich, P. 2020, RNAAS, 4, 171.
- McMullin, J. P., Waters, B., Schiebel, D., Young, W., & Golap, K. 2007, Astronomical Data Analysis Software and Systems XVI (ASP Conf. Ser. 376), ed. R. A. Shaw, F. Hill, & D. J. Bell (San Francisco, CA: ASP), 127.
- Meintjes, P., Odendaal, A., & van Heerden, H. 2015, AcPPP, 2, 86.
- Patterson, J. 1979, ApJ, 234, 978.
- Pelisoli, I., Marsh, T. R., Dhillon, V. S., Breedt, E., Brown, A. J., Dyer, M. J., Green, M. J., Kerry, P., Littlefair, S. P., Parsons, S. G., Sahman, D. I., & Wild, J. F. 2021, MNRAS, in press.
- Perley, R. & Sault, B. 2014, EVLA Memo 178.
- Pretorius, M. L., Hewitt, D. M., Woudt, P. A., Fender, R. P., Heywood, I., Knigge, C., Miller-Jones, J. C. A., Buckley, D. A. H., Worters, H. L., Potter, S. B., & Williams, D. R. A. 2021, MNRAS, 503, 3692.
- Smith, R. C., Dunford, A., & Watson, C. A. 2012, SAIIt (eds. Giovanelli & Sabau-Graziati), 83, 708.
- Thorstensen, J. R. 2020, AJ, 160, 151.
- Torkelsson, U. 2013, IAUS, 290, 145.
- Udalski, A. & Schwarzenberg-Czerny, A. 1989, Act Astron, 39 125.
- van der Laan, H. 1963, MNRAS, 126, 535.
- van der Laan, H. 1966, Nat, 211, 1131.
- Very Large Array Science User Support 2021, science.nrao.edu/facilities/vla/docs/manuals/oss/performance/fdscale
- Watson, C. A., Dhillon, V. S., & Shahbaz, T. 2006, MNRAS, 368, 637.
- Wynn, G. A. & King, A. R. 1995, MNRAS, 275, 9.
- Wynn, G. A., King, A. R., & Horne, K. 1997, MNRAS, 286, 436.

Facilities: VLA

Software: CASA (6.1.2), Julia (1.6.2), Visfit